Electronic Supplementary Information (ESI)

Ti$_3$C$_2$T$_x$ MXene Bonded Perylene Diimide as a Robust Charge Host for Seawater Electrolytes

Sreelakshmi P [a], Soujanya H Goudar [b], Soumyaranjan Behera [b], Kotagiri Venkata Rao*[b], Ambika S*[c], and Narendra Kurra*[b]

[a] Center for Interdisciplinary programs, Indian Institute of Technology Hyderabad, Kandi-502284, Sangareddy, Telangana State, India

[b] Department of Chemistry, Indian Institute of Technology Hyderabad, Kandi-502284, Sangareddy, Telangana State, India

[c] [i]Department of Civil Engineering, [ii] Department of Climate Change, [iii] Greenko School of Sustainability, Indian Institute of Technology Hyderabad, Kandi-502284, Sangareddy, Telangana State, India

* Corresponding authors. E-mail: kvrao@chy.iith.ac.in, ambika@ce.iith.ac.in, narendra@chy.iith.ac.in

Experimental Section

Synthesis of cPDI. Cationic perylene diimide (*c*PDI) was prepared by following the reported literature[1,2]. Briefly, preparation of *c*PDI involves a two-step reaction, where the first step involves preparation of PDI by adding 3,4,9,10-perylene tetracarboxylic dianhydride (1g, 2.55 mmol) and N,N-dimethylethylenediamine (0.89 g, 10.19 mmol) to the imidazole (10 g). This condensation reaction was carried out at 120 °C for 8 h. Thus obtained precipitate was filtered and washed repeatedly with methanol to remove the unreacted imidazole. The filtrant was dried under vacuum at a temperature of 70 °C for 8 h. The estimated yield of PDI was ~ 59% (800 mg). ^{1}H NMR (600 MHz, CDCl$_3$) δ 8.61 (d, J = 7.9 Hz, 4H), 8.54 (d, J = 8.1 Hz, 4H), 4.30 (t, J = 7.0 Hz, 4H), 2.64 (t, J = 7.0 Hz, 4H), 2.32 (s, 12H). (Fig. S1)

The prepared PDI (370 mg, 0.69 mmol) was treated with benzyl bromide (475 mg, 2.77 mmol) at 80 °C in dimethyl formamide (DMF) for 7 h. The resulting reaction mixture was added dropwise to the toluene. The obtained precipitate was filtered and washed several times with toluene. The final product was obtained in reddish brown colour with a yield of 83% (508 mg). ^{1}H NMR (400 MHz, DMSO-d$_6$) 8.83 (d, J= 8.0 Hz, 4H), 8.52 (d, J =7.8 Hz, 4H), 7.72 – 7.64 (m, 4H), 7.61 – 7.51 (m, 6H), 4.76 (s, 4H), 4.65 – 4.60 (m, 4H), 3.76 – 3.57 (m, 4H), 3.20 (s, 12H) (Fig. S2).

Synthesis of Ti$_3$C$_2$T$_x$ MXene. Delaminated Ti$_3$C$_2$T$_x$ MXene was synthesized by selective etching of 'Al' metal from the Ti$_3$AlC$_2$ MAX (particle size $\leq$ 40 µm, Carbon-Ukraine (Y-carbon, Ltd)) phase via top-down wet chemical etching method followed by the delamination step.[3] Wet chemical etching was carried out following the mixed acid method, by adding 1g of Ti$_3$AlC$_2$ MAX phase to an etchant volume of 20 mL containing 12M hydrochloric acid (HCl, Finar), deionized (DI) water and, 49% hydrofluoric acid (HF, Avra) in a volume ratio of 6:3:1 respectively. Etchant solution was taken in a polypropylene bottle and 1 g of MAX phase was slowly added to the etchant solution at room temperature under constant stirring at 400 rpm. Since the etching reaction is exothermic in nature, heat liberation and bubble formation due to gas liberation were observed at the initial stages of the reaction. After a while, the etchant containing MAX was transferred to an oil bath kept at a temperature of 35 °C under continuous stirring for 24 h. The acidic multilayered Ti$_3$C$_2$T$_x$ solution thus obtained was washed using DI water via centrifugation at 3500 rpm for 5 minutes each time. The clear supernatant was discarded and the washing was continued until the pH reached 6-7.

The wet multilayered Ti$_3$C$_2$T$_x$ was mixed with 50 mL of DI water containing 1g of lithium chloride (LiCl, SRL) and kept stirring at a temperature of 35 °C for 24 h. Thus obtained solution was washed using DI water through centrifugation at 3500 rpm for 5 minutes twice and the clear supernatant was discarded. The washing was continued twice by centrifuging at 3500 rpm for 45 minutes until the pH was 6-7 and the supernatant attained a greenish tint, indicating the formation of delaminated dilute dispersion of Ti$_3$C$_2$T$_x$ MXene. The centrifugation process was continued at 3500 rpm for 10 minutes and the dark colloidal supernatant dispersion of delaminated MXene was collected. The delaminated MXene colloidal solution was then filtered over polypropylene filter paper (celgard, pore size – 64 nm, LLC), vacuum dried and mass was noted.

Fabrication of cPDI electrode. *c*PDI electrode was fabricated by mixing *c*PDI, delaminated Ti$_3$C$_2$T$_x$ MXene and polyvinylidene fluoride (PVDF) binder in a ratio of 7:2:1. The consistency of the slurry was maintained using N-methyl pyrrolidone (NMP) as the solvent and was coated over a grafoil current collector using a doctor blade. The fabricated electrode with a typical active material mass loading of ~ 0.5 – 1 mg/cm^2, was then dried at 60 °C in a vacuum oven for 12 h.

Fabrication of cPDI electrode (without Ti$_3$C$_2$T$_x$ MXene). *c*PDI electrode was fabricated by mixing *c*PDI, carbon black and polyvinylidene fluoride (PVDF) binder in a ratio of 7:2:1. The consistency of the slurry was maintained using N-methyl pyrrolidone (NMP) as the solvent and was coated over a grafoil current collector using a doctor blade. The fabricated electrode with a typical active material mass loading of ~ 0.8 – 1 mg/cm^2, was then dried at 60 °C in vacuum oven for 12 h.

Preparation of activated carbon (AC) film. A mixture of 95 wt% of activated carbon powder (YP50F, Kuraray, Japan) and 5 wt% of polytetrafluoroethylene (PTFE, 60 wt% in water) was grounded in a mortar and pestle, to make a slurry by adding a small amount of ethanol. The slurry was rolled into films of thickness ~100-120 µm and kept for drying in a hot air oven at a temperature of 70 °C overnight. The mass loading of the AC films is typically 7 mg/cm^2. The fabricated over-capacitive carbon electrodes were directly used as counter electrodes for three-electrode electrochemical measurements.

Electrochemical measurements:

Cyclic voltammetry (CV), galvanostatic charge-discharge (GCD), and potentiostatic electrochemical impedance spectroscopy (PEIS), and staircase potentio electrochemical impedance spectroscopy (SPEIS) techniques were performed using an SP-150e electrochemical workstation (Biologic, France). All the measurements were done at room temperature. 3 mm diameter electrodes punched from the fabricated *c*PDI electrode (typical

areal mass loading of ~ 0.5-1 mg/cm^2 and thickness of ~ 3 μm) were fixed over a glassy carbon, employed as a working electrode and an overcapacitive AC film as a counter electrode. Three-electrode measurements were carried out in a plastic Swagelok cell with Ag/AgCl (3M KCl) as the reference electrode in 3M NaCl, 3M KCl and 3M MgCl$_2$ aqueous electrolytes.

Calculations. Specific capacity was calculated by integrating the current *vs.* time plots and normalized with respect to the mass of the electrode material. Only the active mass of *c*PDI was considered for the calculation of capacity in all the cases.

$$Specific\ capacity = \frac{1}{m}\int idt$$
(1)

Gravimetric specific capacitance C_m (F/g) was calculated from the CVs by the integration of the discharge portion using the equation,

$$Cm = \frac{1}{Vmv}\int idv$$
(2)

where V is the potential window (V), m is the mass of the active material (mg), v is the scan rate (mV/s) and i is the current (mA).

SPEIS measurements were carried out from a frequency range of 100 kHz to 10 mHz by applying a small sinusoidal voltage of 10 mV while the electrode was held at different DC potentials from a range of -0.9 to 0.2 V (*vs.* Ag/AgCl) in each 50 mV step.

The real capacitance, C$'$ and imaginary capacitance, C$''$ were calculated based on the following equations,

$$C' = \frac{-Z''}{2\pi f|Z|^2}$$
(3)

$$C'' = \frac{Z'}{2\pi f|Z|^2}$$
(4)

where Z' and Z'' are the real and imaginary components of impedance respectively, $|Z|$ is the absolute value of the impedance (Ω) and f is the frequency (Hz).

Phase angle (Φ) was estimated by the following equation,

$$\Phi = -\tan^{-1}\frac{z''(\omega)}{z'(\omega)}$$
(5)

Material Characterization:

X-ray diffractograms were recorded using a powder X-ray diffractometer (PANalytical, Netherlands) with cathode Cu kα, λ=1.5406 Å at 0.13 seconds of dwelling time and 0.013° of step size. JASCO model FTIR-4600 was used for recording the FTIR spectra. Nicolet iS20 Mid-Infrared FT-IR Spectrometer was used for the ATR-FTIR measurement. JASCO model V-770 UV-Vis-NIR spectrophotometer in a screw-capped quartz cell of 10 mm optical path length was used for recording electronic absorption spectra. Fluorescence spectra were recorded using a JASCO model FP-8300 spectrophotometer in a screw-capped quartz cell of 10 mm optical path length. The morphology of the electrode was examined using a scanning electron microscope (SEM) JEOL JIB4700F. METLER TOLEDO laboratory meter with a FiveEasy Plus bench line was used for ionic conductivity measurements. Atomic Force Microscopy (AFM) images were recorded using Bruker Multimode Veeco8. The concentration of *c*PDI spray coated on silicon substrate for SEM is 0.1 mM in DI water.
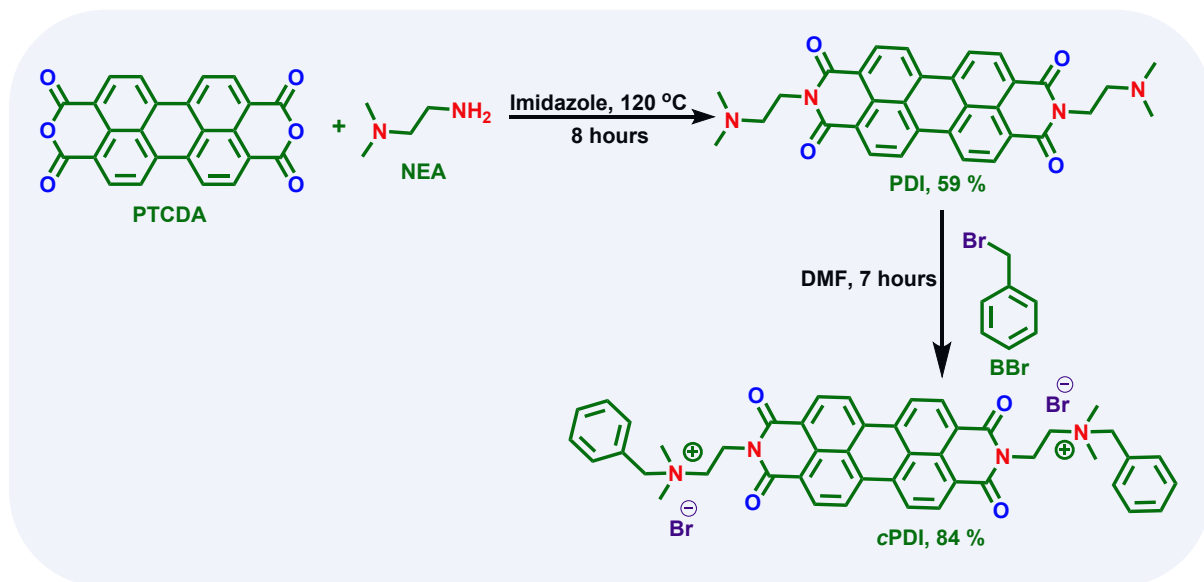
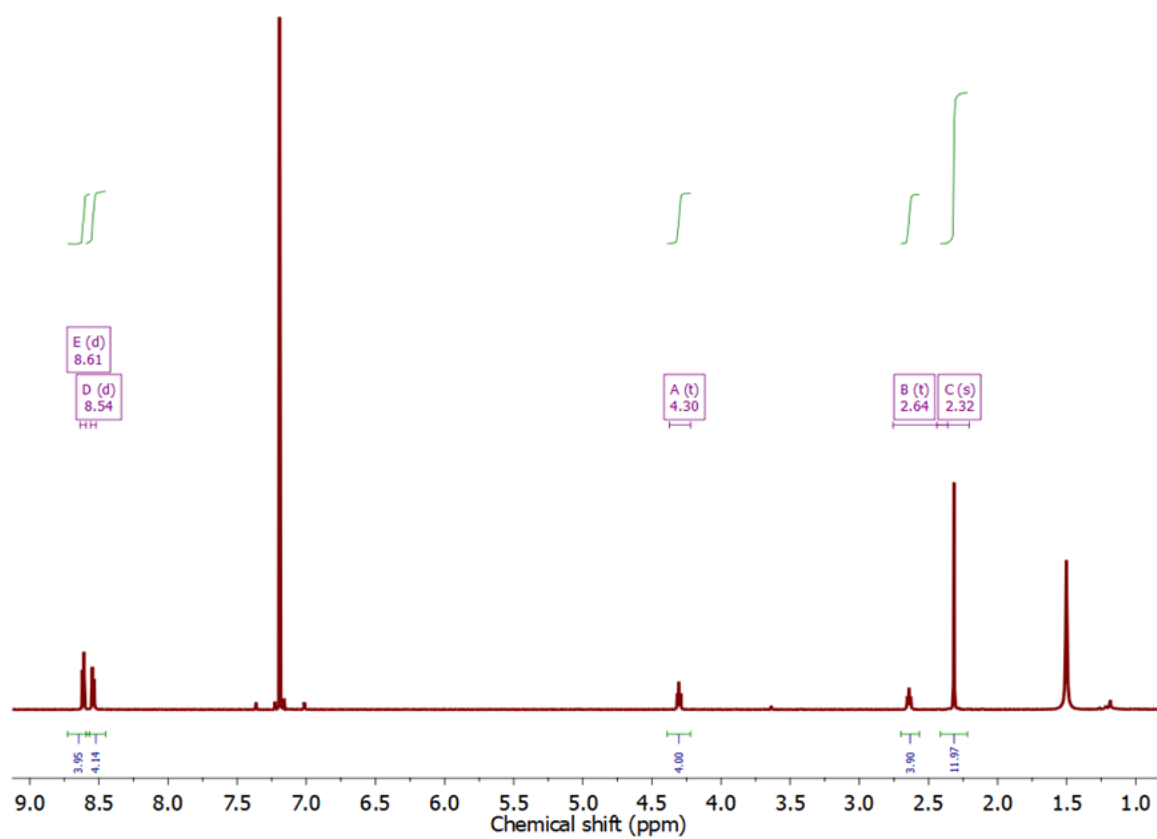**Scheme 1.** Schematic illustration of the synthesis of *c*PDI from PTCDA.
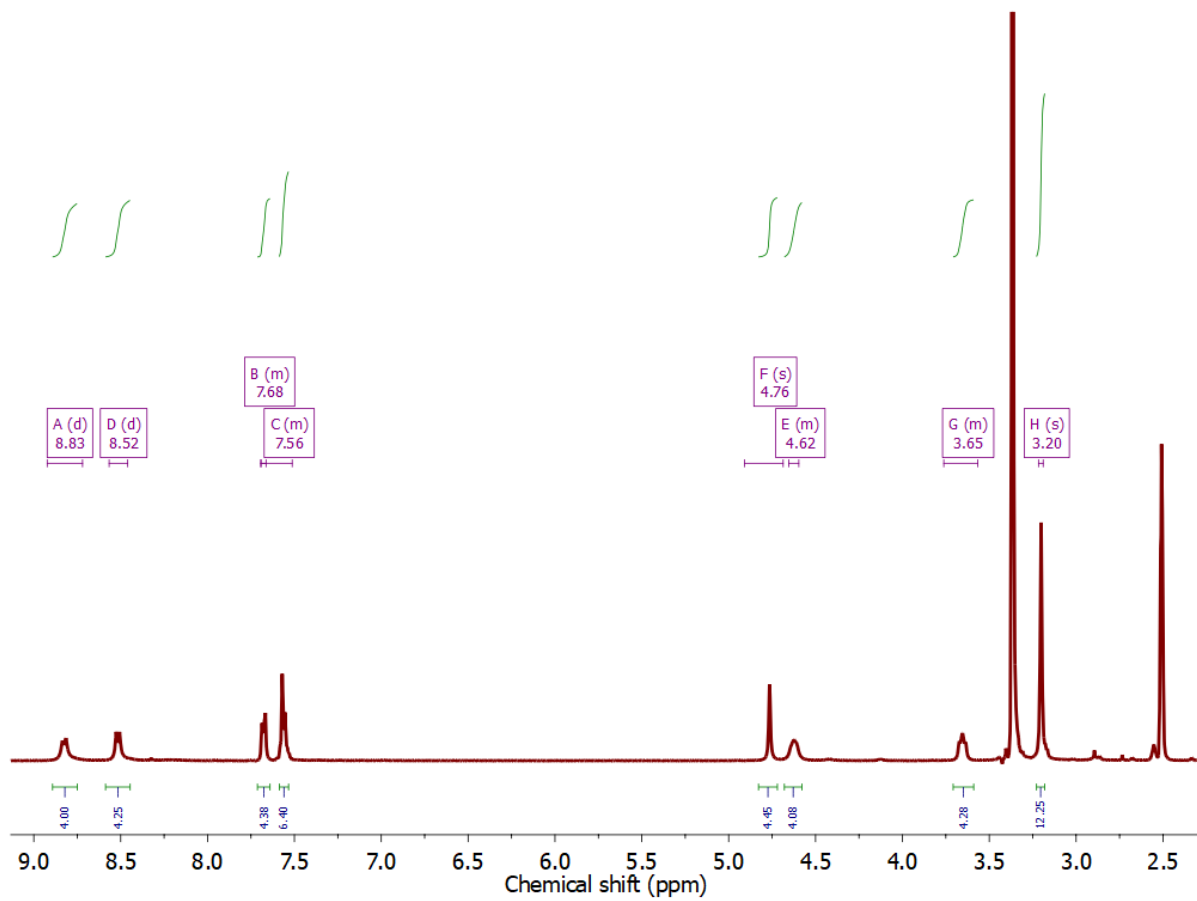
Fig. S1. ¹H-NMR spectrum of PDI.

Fig. S2. ¹H-NMR spectrum of *c*PDI.

Fig. S3. FTIR spectrum of *c*PDI**.** The peaks at 1696 cm^{-1} and 1656 cm^{-1} correspond to the carbonyl (C=O) group, 1591 cm^{-1} to the aromatic C=C, 1254 cm^{-1} to the C-N bond, 1044 cm^{-1} to the C-H bending and the broad peak at 3400 cm^{-1} corresponds to the -OH bond of absorbed

water molecules.

Fig. S4. (a) Field emission scanning electron microscopy (FE-SEM) micrograph of *c*PDI electrode over a large area. (b) Atomic force microscopy (AFM) topography of *c*PDI electrode and the *z*-profile corresponding to the white line as shown in the AFM topography.

Fig. S5. (a) X-ray diffractograms of cPDI (brown), $Ti_3C_2T_x$ MXene (grey) and cPDI electrode (blue). (b) Expanded X-ray patterns of $Ti_3C_2T_x$ MXene in pristine MXene (grey) and cPDI electrodes (blue) showing the (002) peak. (c) Fourier transformed infrared (FTIR) spectra of cPDI (brown) and cPDI electrode (blue).

X-ray diffractograms were employed to confirm the presence of $Ti_3C_2T_x$ MXene and cPDI in the cPDI electrode. The (002) peak of pristine $Ti_3C_2T_x$ MXene at $2\theta \sim 6.6°$ and the prominent peak of cPDI at $2\theta \sim 26.30°$ was observed in the X-ray patterns. Further, the hydrogen bonding interactions between the -OH surface terminations of $Ti_3C_2T_x$ MXene and the carbonyl groups of cPDI were probed through Fourier-transformed infrared (FTIR) spectroscopy. The peaks at 1696 and 1656 cm^{-1} for cPDI are due to the asymmetric and symmetric stretching frequencies respectively for the carbonyl groups. The shift in the frequencies from 1696 to 1691 cm^{-1} for asymmetric stretching and from 1656 to 1649 cm^{-1} for symmetric stretching for the cPDI electrode confirms the plausible hydrogen bonding interactions. A respective shift of 5 cm^{-1} and 7 cm^{-1} in asymmetric and symmetric stretching frequencies accounts for the small fraction of bonding that is present between materials in addition to the blending. In general, the physical interaction between cPDI and $Ti_3C_2T_x$ MXene confirms the blending of these two materials. Moreover, the shift in frequencies of carbonyl peaks in the FTIR spectra confirms the plausible hydrogen bonding interactions between the two materials as well.
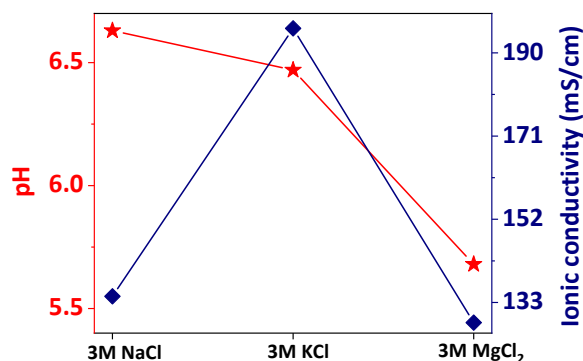
8

Fig. S6. pH and ionic conductivity (mS/cm) values of 3M NaCl, 3M KCl and 3M MgCl$_2$.
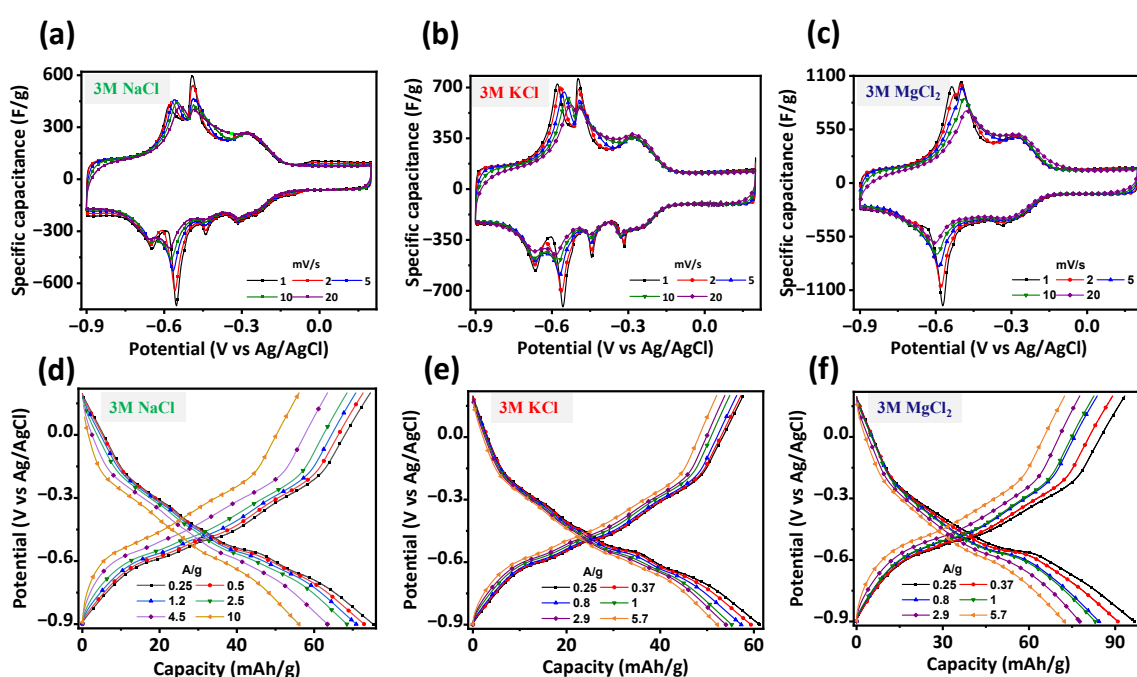

Fig. S7. Cyclic voltammograms of cPDI electrode in (a) 3M NaCl (b) 3M KCl and (c) 3M MgCl$_2$ at various scan rates from 1 to 20 mV/s. GCD profiles of cPDI electrode in (d) 3M NaCl (e) 3M KCl and (f) 3M MgCl$_2$ at different current densities.

Two distinct peaks of charge storage can be observed for monovalent ions (Na$^+$ and K$^+$) while only a single redox peak for bivalent ion (Mg^{2+}) within the same potential window at scan rates > 1 mV/s. However, both monovalent and divalent ions exhibit two peaks within the potential range of -0.6 to -0.3 V (vs. Ag/AgCl) at a scan rate of 1 mV/s. This signifies that energetically equivalent yet distinguishable carbonyl sites are identified at charging time scales of 18 minutes. However, for monovalent ions, these distinguishable carbonyl sites are observed until charging time scales of a few tens of seconds. The way the carbonyl groups are anchored may generate sites with two different surroundings, but energetically equivalent sites in the material.
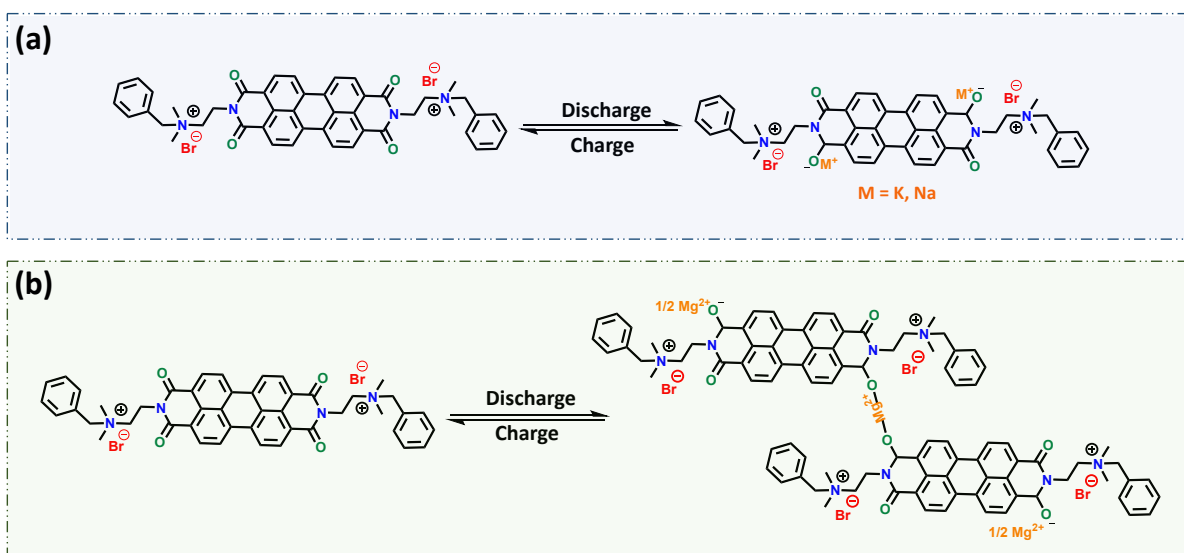
Scheme 2. Schematic illustration representing the plausible reversible electrochemical redox mechanism of *c*PDI (a) for monovalent metal ions Na^+ and K^+ (b) for divalent metal ion Mg^{2+}.

Carbonyl group is the main redox functional group that participates in the Faradaic charge storage mechanism.[6–9] It is well known that whether it is a small molecule or polymeric diimides, apparently charge storage mechanism is similar. In the case of monovalent ions, trans-positioned carbonyl groups attach the metal ions by transferring two electrons per formula unit. Whereas for divalent metal ions, bridging of the divalent cation between the same side carbonyl groups with subsequent transfer of two electrons per formula unit.[7,10]
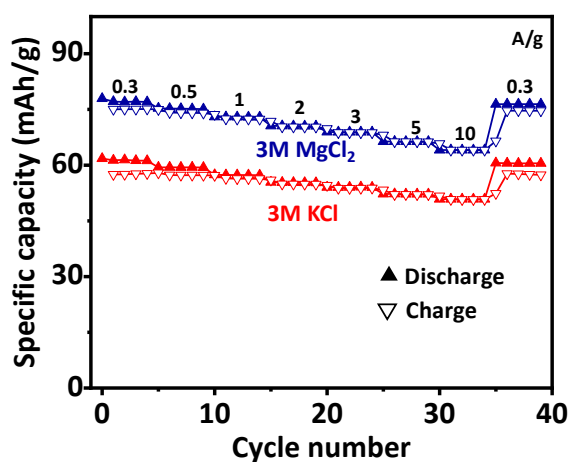

Fig. S8. Rate performance of *c*PDI electrode in 3M MgCl$_2$ and 3M KCl at different current densities of 0.3, 0.5, 1, 2, 3, 5, 10 and 0.3 A/g.
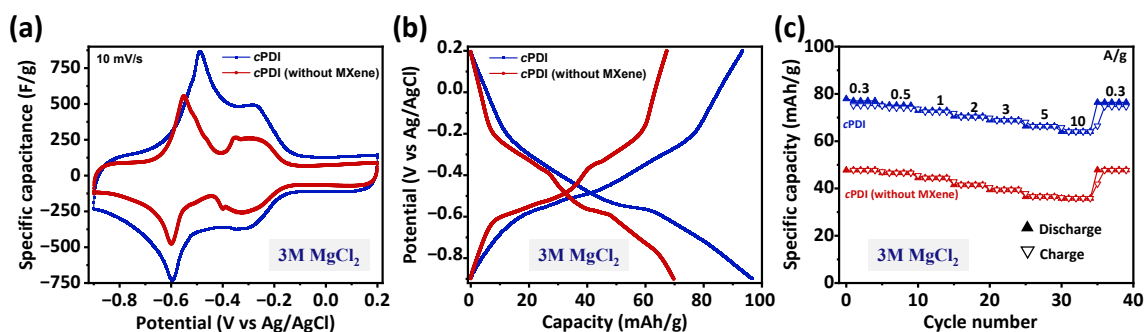
Fig. S9. Comparison of electrochemical performance of *c*PDI with and without bonding to Ti$_3$C$_2$T$_x$ MXene in 3M MgCl$_2$ electrolyte. (a) Cyclic voltammograms at a scan rate of 10 mV/s. (b) Galvanostatic charge-discharge profiles at a current density of 0.25 A/g. (c) Rate performance at different current densities of 0.3, 0.5, 1, 2, 3, 5, 10 and 0.3 A/g.

As observed, Ti$_3$C$_2$T$_x$ MXene is certainly providing better charge transport pathways for carbonyl redox centers of *c*PDI. MXene makes the *c*PDI a highly reversible electrochemical system, obeying the Nernstian behaviour.
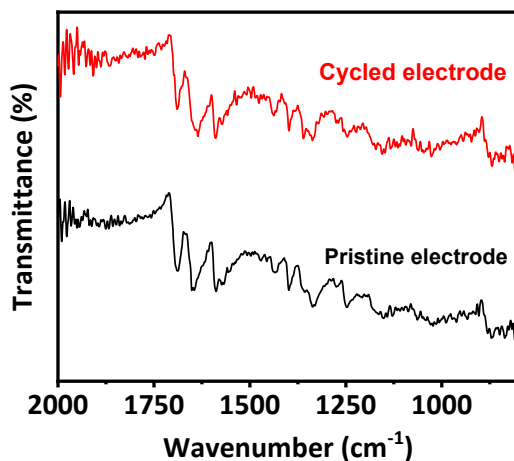

Fig. S10. FTIR of pristine *c*PDI electrode (black) and ex-situ FTIR after cycling (red) in 3M MgCl$_2$ electrolyte.
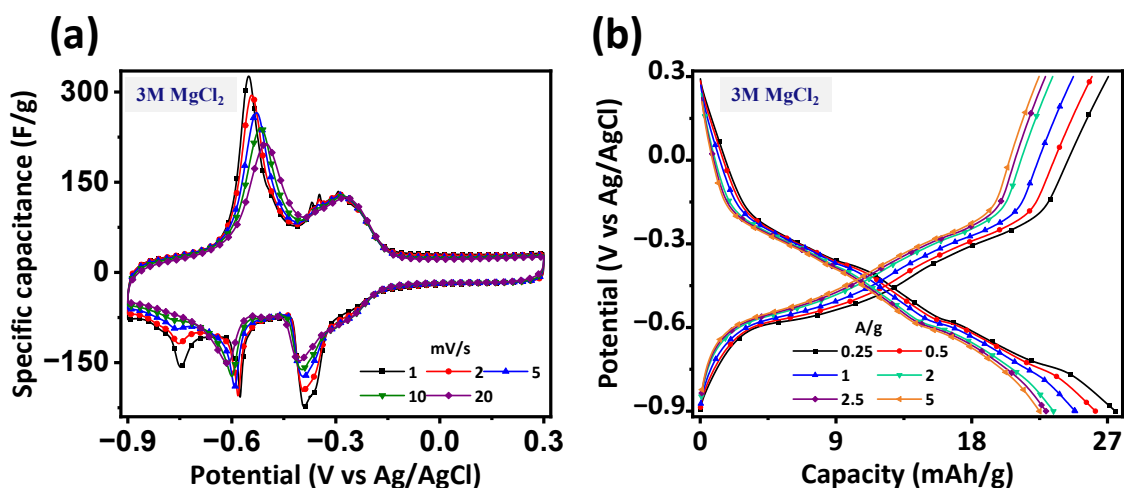
Fig. S11. (a) Cyclic voltammograms and (b) GCD profiles of *c*PDI electrode with multilayered Ti$_3$C$_2$T$_x$ MXene as conductive additive in 3M MgCl$_2$.
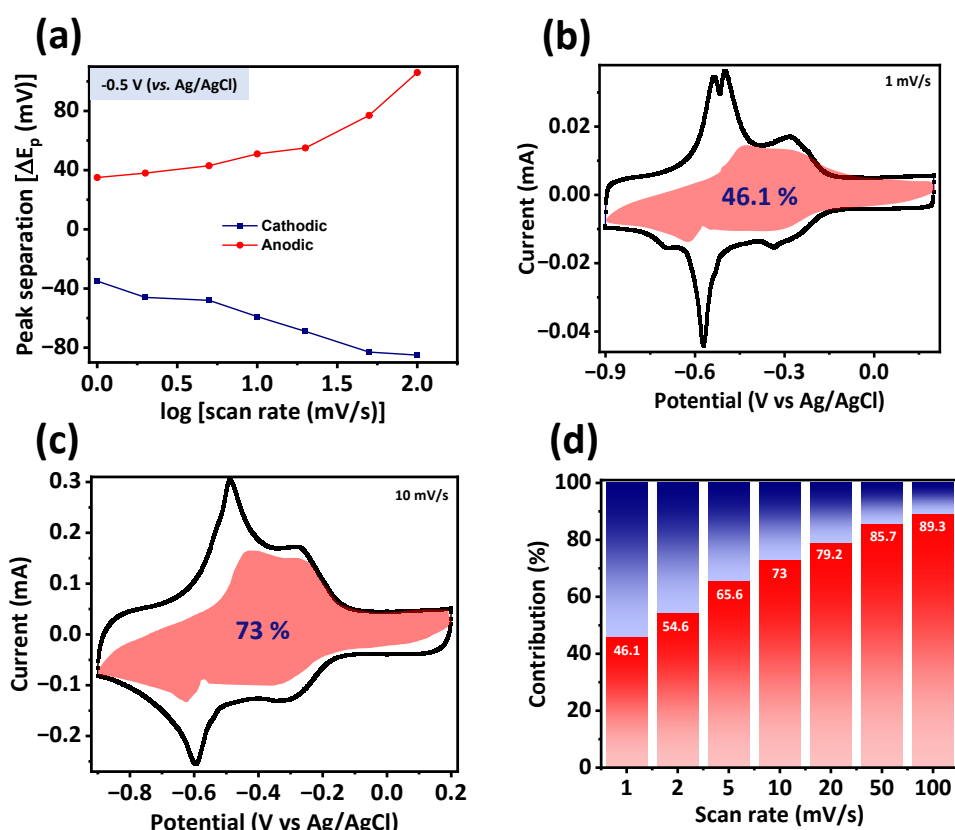

Fig. S12. (a) Trumpet plot with peak separation (ΔE_p) plotted against *log* (scan rate) for varying scan rates from 1 to 100 mV/s for the potential at -0.5 V (*vs.* Ag/AgCl). Contribution of capacitive controlled processes (marked with the light red area) to the overall charge computed at (b) 1 mV/s (slow) and (c) 10 mV/s (fast) scan rates (d) ratio between the contributions of capacitive (red) and diffusion-controlled (blue) for varying scan rates from 1 to 100 mV/s.
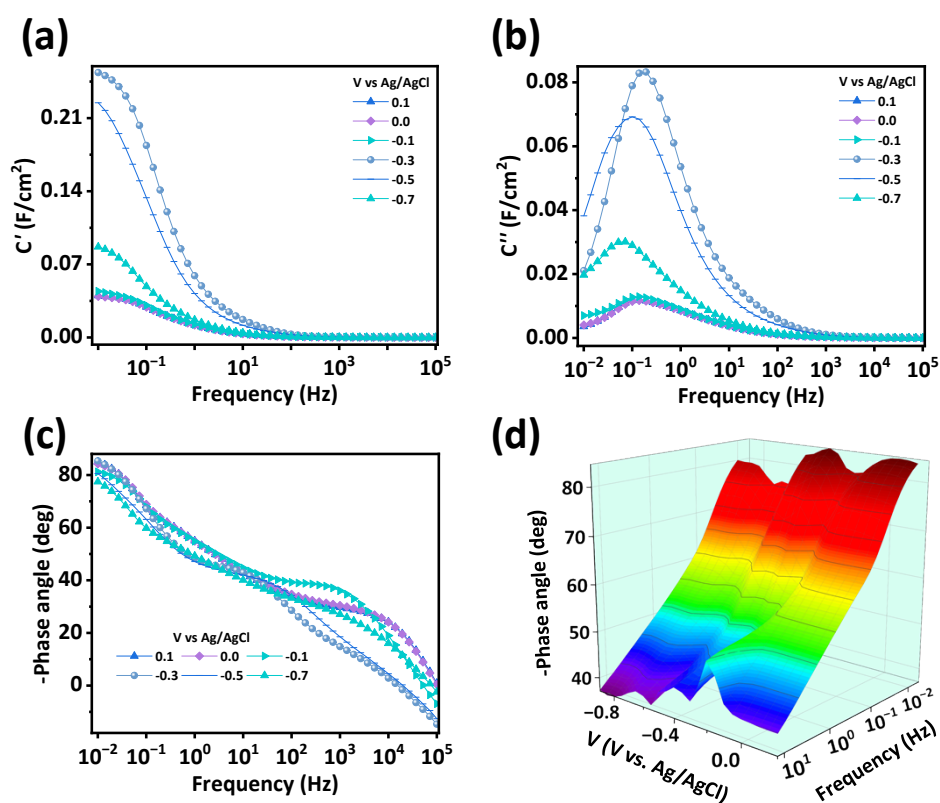
Fig. S13. 2D Bode plots of (a) real capacitance (C′), (b) imaginary capacitance (C″) and (c) phase angle (∅) as a function of frequency. (d) 3D Bode map of phase angle (∅)-potential-frequency.

The maximum value of C′ observed for the potentials ~ -0.3 V and ~ -0.5 V (*vs.* Ag/AgCl) (Fig. S13a, ESI), validates the redox peaks at the corresponding potentials observed in the cyclic voltammogram. Besides, the inverse of frequency (*f*) at the peak value of imaginary capacitance (C″) provides the relaxation time constant ($\tau_0 = 1/f$). In 3M MgCl$_2$, the variation of the peak value of C″ with different potentials applied can be observed in Fig. S13b, ESI. The relaxation time constant was calculated to be 5 and 10 seconds at potentials of -0.3 V and -0.5 V (*vs.* Ag/AgCl), respectively. Such kind of time scales represent the dominant redox reactions that are happening across the electrode|electrolyte interface and substantiate the potential dependence of redox charge storage across the interface.

References

1   S. H. Goudar, D. S. Ingle, R. Sahu, S. Kotha, S. K. Reddy, D. J. Babu and V. R. Kotagiri, *ACS Appl. Polym. Mater.*, 2023, **5**, 2097–2104.

2   Y. Jiao, K. Liu, G. Wang, Y. Wang and X. Zhang, *Chem. Sci.*, 2015, **6**, 3975–3980.

3   M. Alhabeb, K. Maleski, B. Anasori, P. Lelyukh, L. Clark, S. Sin and Y. Gogotsi, *Chem. Mater.*, 2017, **29**, 7633–7644.

4   M. Shekhirev, C. E. Shuck, A. Sarycheva and Y. Gogotsi, *Prog. Mater. Sci.*, 2021, **120**, 100757.

5   H. Zhao, Y. Zhang, H. Xu, Z. He, Z.-L. Zhang and H. Zhang, *Tetrahedron*, 2015, **71**, 7752–7757.

6   A. Nimkar, G. Bergman, E. Ballas, N. Tubul, N. Levi, F. Malchik, I. Kukurayeve, M. S. Chae, D. Sharon, M. Levi, N. Shpigel, G. Wang and D. Aurbach, *Angew. Chemie Int. Ed.*, 2023, **62**, e202306904.

7   L. Chen, J. L. Bao, X. Dong, D. G. Truhlar, Y. Wang, C. Wang and Y. Xia, *ACS Energy Lett.*, 2017, **2**, 1115–1121.

8   S. Yuan, X. Huang, T. Kong, L. Yan and Y. Wang, *Acc. Chem. Res.*, 2024, **57**, 1550–1563.

9   S. K. Lee, Y. Zu, A. Herrmann, Y. Geerts, K. Müllen and A. J. Bard, *J. Am. Chem. Soc.*, 1999, **121**, 3513–3520.

10   S. Gheytani, Y. Liang, F. Wu, Y. Jing, H. Dong, K. K. Rao, X. Chi, F. Fang and Y. Yao, *Adv. Sci. (Weinheim, Baden-Wurttemberg, Ger.*, 2017, **4**, 1700465.